ISSN (Print) 1226-1750
ISSN (Online) 2233-6656
Journal of Magnetics 22(2), 306-314 (2017) https://doi.org/10.4283/JMAG.2017.22.2.306

An Investigation of Induction Motor Saturation under Voltage Fluctuation Conditions

Morteza Ghaseminezhad[1], Aref Doroudi[1]*, Seyed Hossein Hosseinian[2], and Alireza Jalilian[3]

[1]*Electrical Engineering Department, Shahed University, Tehran, Iran*
[2]*Electrical Engineering Department, Amirkabir University of Technology (AUT), Tehran, Iran*
[3]*Electrical Engineering Department, Iran University of Science & Technology (IUST), Tehran, Iran*

(Received 10 September 2016, Received in final form 15 March 2017, Accepted 16 March 2017)

Nowadays power quality effects on induction motors have gained significant attention due to wide application of these motors in industry. The impact of grid voltage fluctuations on the induction motor behavior is one of the important issues to be studied by power engineers. The degree of iron saturation is a paramount factor affecting induction motors performance. This paper investigates the effects of voltage fluctuations on motor magnetic saturation based on the harmonic content of airgap flux density by finite element method (FEM). It is clarified that the saturation harmonics under normal range of voltage fluctuations have not changed significantly with respect to pure sinusoidal conditions. Experimental results on a 1.1 kW, 380 V, 50 Hz, 2 pole induction motor are employed to validate the accuracy of the simulation results.

Keywords : induction motor, finite element method, voltage fluctuation, magnetic saturation

1. Introduction

Recently voltage fluctuation is increasingly getting attention due to many undesirable effects making on sensitive residential and industrial loads. The most famous effect of the voltage fluctuations can be realized in the light fluctuations of lighting systems. Flicker frequencies in the range of 0.05 to 35 Hz can cause perceptible flicker [1]. Induction motors are widely used in many industrial, commercial and residential applications because of various techno-economic advantages [2, 3]. It is estimated that more than 50 % of the world's generated electrical energy is consumed by electric machines (mainly by induction motors) [4]. Subsequently, it is important to study the effects of any disturbance such as voltage fluctuations on the behavior of induction motors. The effect of voltage fluctuations on currents, speed, torque and efficiency of induction machines was studied in [5-10]. A quick survey of the literature shows that in most cases, simulations based on the d-q frame model are applied to show induction motor characteristics under voltage fluctuation conditions. However, investigation about saturation of iron parts due to the voltage fluctuations has not been performed yet. Saturation effects on the steady state performance of induction motor related to air gap flux harmonics were described for the first time in [11] and [12].

The saturable parts of an induction machine are stator teeth, rotor teeth, and stator and rotor cores. Under highly saturated conditions, the resultant air-gap flux density wave may be either flat-topped or peaked, related to teeth or core saturation [13]. In most machines, the tooth is more saturated than the core since the cross section area of iron in the yoke is much greater than in the tooth where a much higher flux density exists. High saturation may also occur when a machine operates at voltages higher than the rated value, or at frequencies lower than the nominal value. The disadvantages of high saturation are high magnetizing current, low power factor, and harmonic currents feeding back to the line [11]. Supply sinusoidal voltage with subharmonics can cause a significant flux peak increase, resulting in eventual saturation of the motor, as discussed in [14]. Voltage fluctuations can be considered as superposition of a subharmonic and an interharmonic component. The investigation of saturation depth of induction motors in the presence of the normal range of voltage fluctuations is the major contribution of this paper. This is carried out by FEM simulations and based on the saturation harmonics of airgap flux density. The motor is supplied with fluctuated voltages considering nonlinear BH curve to investigate the

*Corresponding author: Tel: +98-21-5121-2035
Fax: +98-21-5121-2035, e-mail: doroudi@shahed.ac.ir

saturation depth of induction motor. Finally, experimental results are provided to validate the simulation results through this paper.

2. Voltage Fluctuations

Due to as load characteristics, the voltage fluctuations can be cyclic or stochastic. Nevertheless, in a short period, the voltage fluctuations can be estimated by an amplitude modulation formula represented by the following equation [5]:

$$v_a(t) = V_p\Big(1 + \sum_{j=1} k_j \sin(2\pi f_j t)\Big)\cos(2\pi f_b t) \quad (1)$$

where f_b is the fundamental frequency of ac voltage, f_j is the modulation (flicker) frequency, V_p is the line to neutral peak voltage and k_j is the modulation depth. In this way, the source voltage is assumed a sinusoidal amplitude modulated source and sinusoids superimposed on the fundamental voltage are assumed to be the fluctuating components. With one modulation frequency and one modulation depth, the line to neutral voltage of phase A is defined as:

$$v_a(t) = V_p(1 + k_m \sin(2\pi f_m t))\cos(2\pi f_b t) \quad (2)$$

In the balanced systems, the other phases can be given in the same manner except in that the phase angle of fundamental frequencies in the other two phases should be modified by −120 and +120, respectively. Heavy loads such as arc furnaces whose power demands are rapidly variable and light loads such as copying machines that are intermittent in time can lead to voltage fluctuations [15].

3. Finite Element Method

The finite element method (FEM) grows as the most advantageous numerical analysis tool to study and design of electric machines. Finite element method with addition of time-stepping can provide quite accurate prediction of transient performance of electrical machines [16]. The advantage of this technique is that magnetic saturation and space distribution of stator and rotor windings can be taken into account. Finite element method with addition of time-stepping can provide quite accurate prediction of transient performance of electrical machines [17]. In this paper, time-stepping FEM is used for the analysis of the motor magnetic field. The governing equation for two-dimensional (2-D) FE analysis is given by [18]:

$$\frac{\partial}{\partial x}\Big(\frac{1}{\mu}\frac{\partial A}{\partial x}\Big) + \frac{\partial}{\partial y}\Big(\frac{1}{\mu}\frac{\partial A}{\partial y}\Big) = \sigma\frac{\partial A}{\partial t} - J_0 \quad (3)$$

Table 1. motor parameters.

description	value	description	value
specification			
Nominal power	1100 W	Nominal speed	2825 rpm
Frequency	50 Hz	Nominal voltage	220 V
stator			
number of stator slot	24	core length	80 mm
inner diameter	62 mm	stacking factor	0.95
outer diameter	120 mm	connection type	wye
number of phase	3	number of pole	2
conductor per slot	70	strands per conductor	1
rotor			
number of rotor slot	18	core length	80 mm
Inner Diameter	24.5 mm	stacking factor	0.95
outer diameter	61 mm	endring width	10 mm
material	aluminum	endring height	10 mm

where μ and σ are the permeability and conductivity of the materials respectively. A is the z component of magnetic vector potential and J_0 is stator windings exciting current density.

The design parameters of the motor (listed in Table 1) are applied in FE analysis. This motor has a one-layer lap stator winding, arranged for three phases and two poles in 24 stator slots. The rotor is an aluminum cage with 18 slots. The rotor slots are not skewed. The stator and rotor cores are made of steel sheet laminations with 3.5 % silicon and 0.5 mm thickness. The nonlinear characteristic of the core materials has been taken into account in the finite element analysis. Three balanced fluctuated voltages are applied on the motor terminals by use of external circuits.

4. Analysis of Magnetic Saturation under Voltage Fluctuation Conditions

In this section, effects of voltage fluctuations on the saturation mode of operation of induction motor have been investigated by FE analysis. In this way, the motor is first supplied with a pure sinusoidal voltage considering both linear and nonlinear BH curves and stator current and flux density harmonics are compared. This has been done to distinguish between saturation harmonics and mmf space harmonics. Subsequently, the motor will be supplied with fluctuated voltages considering nonlinear BH curve to investigate the saturation depth of induction motor under voltage fluctuation conditions.

4.1. Pure Sinusoidal Supply; Linear and Non-Linear BH Curve

In this section, the flux density harmonics of the induction motor for linear and nonlinear B-H curves are first obtained and then the motor characteristics such as airgap flux density and stator tooth flux under saturation mode are investigated. The constant permeability of the linear BH curve is assumed to be $\mu_r = 1500$. Figure 1 shows the instantaneous variations of flux density and their frequency spectrums at one point in the middle of airgap, lying directly under a stator tooth (hereafter called point A) for both linear and nonlinear BH curves using FE simulation. The figure depicts that the peak value of flux density is slightly bigger than for the case of linear BH curve whereas the shape of flux density is approximately the same for both linear and nonlinear BH curves.

According to [19], the principal slot harmonics of the air gap flux density can be expressed as:

$$Psh = \left(\frac{gR}{P}(1-s) \pm 1\right) f_b \qquad (4)$$

where P is the number of motor pole pairs, R is the number of rotor slots, s is the slip, f_b is the supply frequency and g is an integer (1, 2, 3, etc.).

In the simulated induction motor, number of rotor slots R=18 and its rotor speed at rated load is n_r = 2880[rpm], synchronous speed is $n_s = \frac{60 f_b}{P} = 3000$, then the slip is obtained as $s = \frac{3000 - 2880}{3000} = 0.04$. Therefore, slot harmonics can be easily derived from (4).

However, in the nonlinear case, there are two components at the frequencies of 150 and 250 Hz due to saturation that are not observed for the linear case. These harmonics are called saturation harmonics since they are produced directly by magnetic saturation and are not excited by mmf harmonics in the air gap [11]. This can be confirmed by the flux density spectrum shown in Fig. 1, where the third harmonic produced by saturation is about 0.9 % (assuming the fundamental as base). The magnitude of high order saturation harmonics are insignificant and can be ignored.

There are two other types of harmonics in induction motors. Firstly, the time harmonics which are created due to non-ideal power supplies. Secondly, the space harmonic that is made as a result of non-ideal winding distribution and slotting. Saturation harmonics are different from the time and space harmonics in the case of rotating speed. The saturation harmonics rotate in the air-gap with the same speed and direction as the fundamental frequency, whereas the time and space harmonics create rotating fields with the speed of integer and non-integer multiple of the supply fundamental frequency, respectively.

In order to recognize saturation effects, the motor has been tested at 50 % over voltage (without fluctuations) to produce substantial saturation. The stator tooth flux and the airgap flux density (at point A) as well as their frequency spectrums, obtained from FEM simulation, are illustrated in Fig. 2. It is obvious that the saturation of stator and rotor teeth causes the stator flux wave to be flat-topped. The third harmonic of flux density (the 150 Hz component) is about 3.4 % of the fundamental component.

As mentioned, the saturation harmonics rotate in the air-gap with the same speed as the fundamental frequency. Hence, saturation harmonic fluxes induce voltages in the stator winding at frequencies which are multiples of the

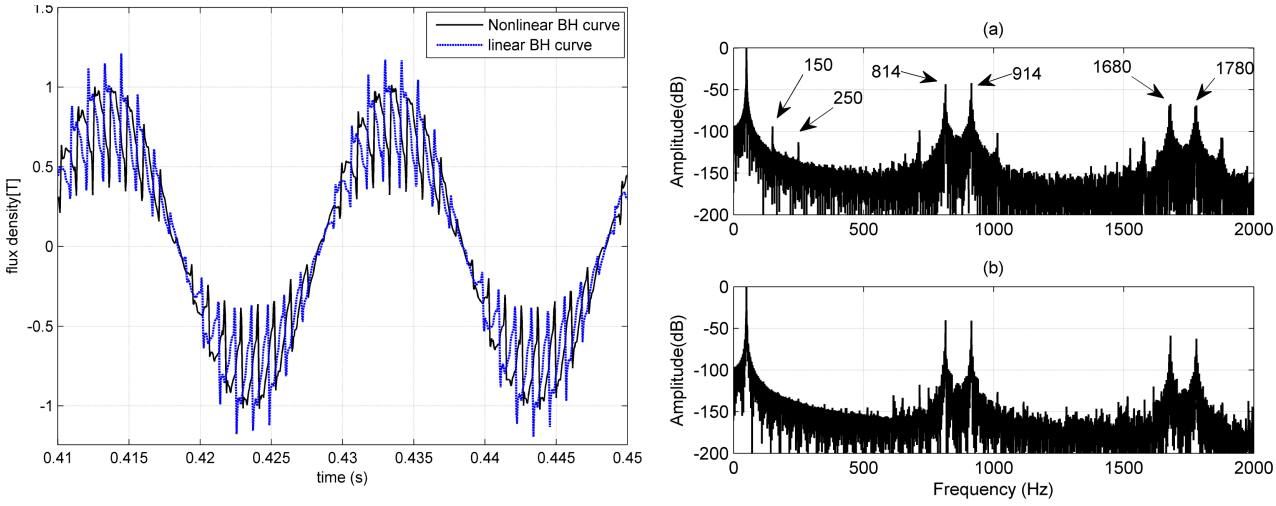

Fig. 1. (Color online) Magnetic flux density curves (left) and their frequency spectrums (right) in normal condition at point A in two cases; (a) nonlinear, (b) linear B-H curve.

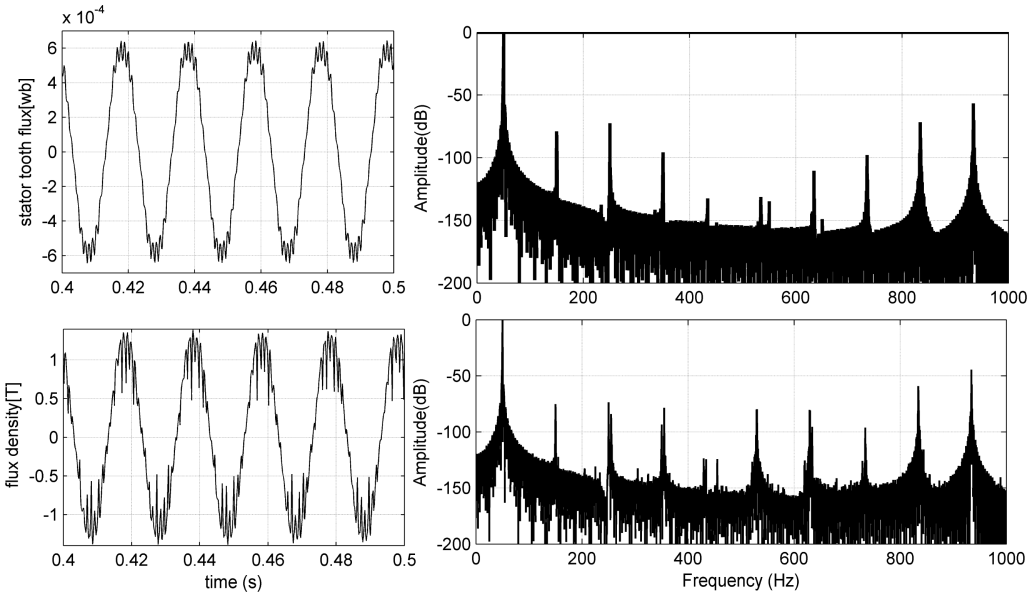

Fig. 2. Stator tooth flux and the magnetic flux density of one point in the middle of airgap under stator tooth as well as their frequency spectrum at 50 % over voltage obtained by FEM.

supply fundamental frequency. The stator winding of the simulated motor is star-connected. Therefore the triplen harmonic voltages in each phase are co-phasal and can be ignored. Non-triplen harmonic voltages cause harmonic currents in the supply system. However, as result of the high impedance of the supply system and the motor at harmonic frequencies, these currents are usually small. They produce small mmf waves rotating in the air gap at multiples of the synchronous speed. The stator current of phase A and corresponding frequency spectrum with 50 % over voltage are shown in Fig. 3. It is clear that the stator current has components in 250(h = 5), 350(h = 7), 550(h = 11), 650(h = 13) Hz. As expected, the triplen harmonic currents have very small magnitude. It can be seen that, high saturation has induced harmonics in both the stator current and air-gap flux. One of the most important facts regarding the saturation harmonics is that they all rotate at the same angular speed as the fundamental component. These rotating harmonics induce rotor current. Hence, all the rotor-induced saturation current harmonics have the same slip and produce useful torque in squirrel-cage machines [13, 20] and create a ripple in the total torque [21].

4.2. Voltage Fluctuation Conditions; Nonlinear BH Curve

In this section, magnetic saturation under voltage fluc-

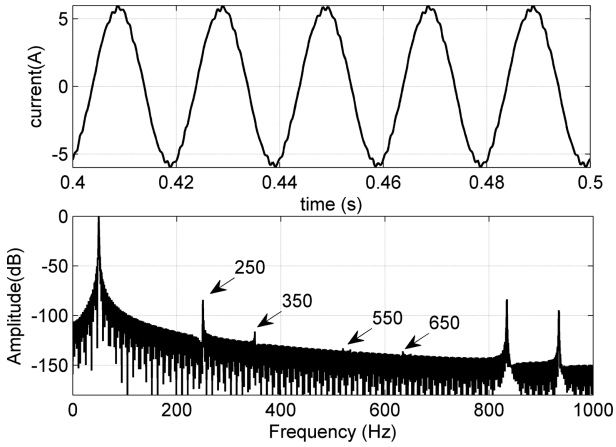

Fig. 3. Current of phase "A" and its frequency spectrum at 50 % over voltage.

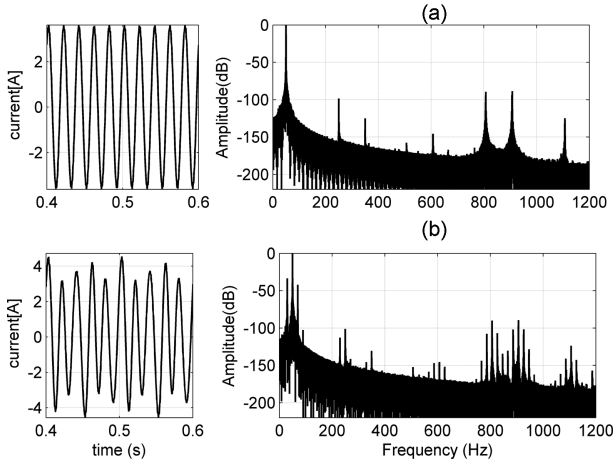

Fig. 4. Current under normal and voltage fluctuation conditions obtained by FEM (f_m = 20 Hz and k = 0.05).

tuation conditions is investigated.

Figure 4 shows the stator current and its frequency spectrum obtained by FEM in two cases; normal operation (part a) and under voltage fluctuation conditions with modulation frequency of 20 Hz and modulation depth of 0.05 (part b). In the normal condition, the EMF frequencies induced in stator current of induction motor are a function of pole numbers and can be expressed as equation (4) [19]. According to the simulated results and as it is shown in Fig. 4(a), the induced frequency components in stator current spectrum of induction motor under rated load and normal condition with s = 0.04 are 814, and 914 Hz which is corresponding with g = 1.

In fact, the frequencies 814 and 914 Hz are the principal slot harmonics called PSH_1 and PSH_2 [19]. The frequency components produced due to B-H characteristics can be observed at 250 and 350 Hz in stator current spectrum shown in Fig. 4(a). As it is seen in Fig. 4(b), the same fundamental voltage magnitude of upper and lower components establishes different magnitudes of current at corresponding frequencies. This occurs due to smaller effective input impedance of the motor at lower frequency (30 Hz) compared with upper frequency (70 Hz). Also, relatively negligible current components at frequencies of $f_b \pm 2jf_m$ (j = 1, 2, 3, ...) are seen in the figure.

The variations of stator tooth flux versus time and its frequency spectrum, in two cases; normal operation and under voltage fluctuation conditions have been illustrated in Fig. 5. The voltage fluctuation with modulation depth of 5 % makes the teeth flux component with amplitude about 7 % of the fundamental component. As it is seen, in addition to the fundamental component, its sideband components (the lower and upper) are clearly shown in the figure. Furthermore, at 814, 914 slot harmonics and

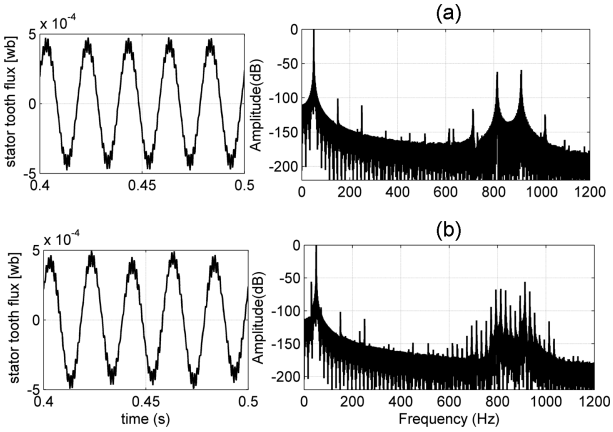

Fig. 5. Stator tooth flux and its frequency spectrum in two cases; (a) normal, (b) under fluctuated voltages (f_m = 20 Hz and k = 0.05).

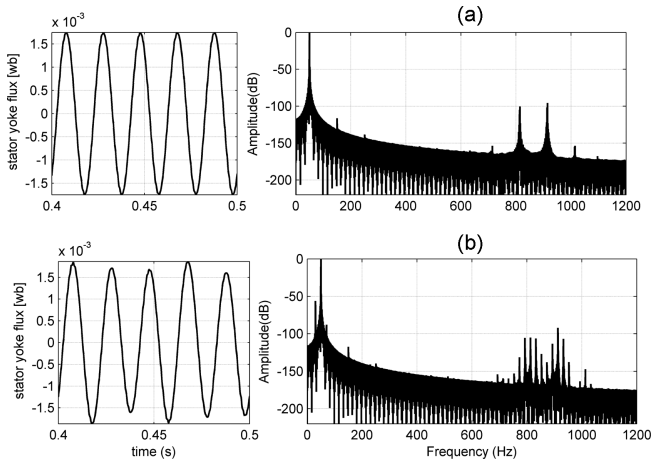

Fig. 6. Stator yoke flux and its frequency spectrum in two cases; (a) normal, (b) under fluctuated voltages (f_m = 20 Hz and k = 0.05).

their sideband components with significant amplitudes are obviously seen in the frequency spectrum.

The variations of stator yoke flux versus time and its frequency spectrum, in two cases; normal operation and under voltage fluctuation conditions have been illustrated in Fig. 6.

Voltage fluctuations with modulation depth of 5 % create the yoke flux component with amplitude about 7 % of the fundamental component. As it can be seen in Fig. 5 and 6, the amplitudes of saturation harmonics under voltage fluctuation conditions have not changed significantly (as compared to the normal operation).

The instantaneous flux density in normal operation (pure sinusoidal supply) and under voltage fluctuation conditions at point A are compared as shown in Fig. 7. As it is seen, flux density peak value under fluctuated conditions is slightly higher than that of pure sinusoidal supply. It is also seen that the flux density during voltage fluctuation conditions has some extra frequency components as compared to pure sinusoidal supply. These new components appear at sidebands of fundamental frequency $f_b \pm f_m$ and at sidebands of individual harmonics ($hf_b \pm 2jf_m$ where h is the harmonic number and j is an integer) and may affect the peak value of the flux density. The maximum effect of each component is proportional to its amplitude. The normalized flux density maximum increase is expressed as:

$$\Delta B_m = \sum_{i=1}^{n} \left(\frac{B_{spi}}{B_s} + \frac{B_{sni}}{B_s} \right) \tag{5}$$

Where ΔB_m is the normalized maximum increase in the peak value of flux density, B_s is the amplitude of fundamental component and B_{spi} and B_{sni} are the amplitudes of

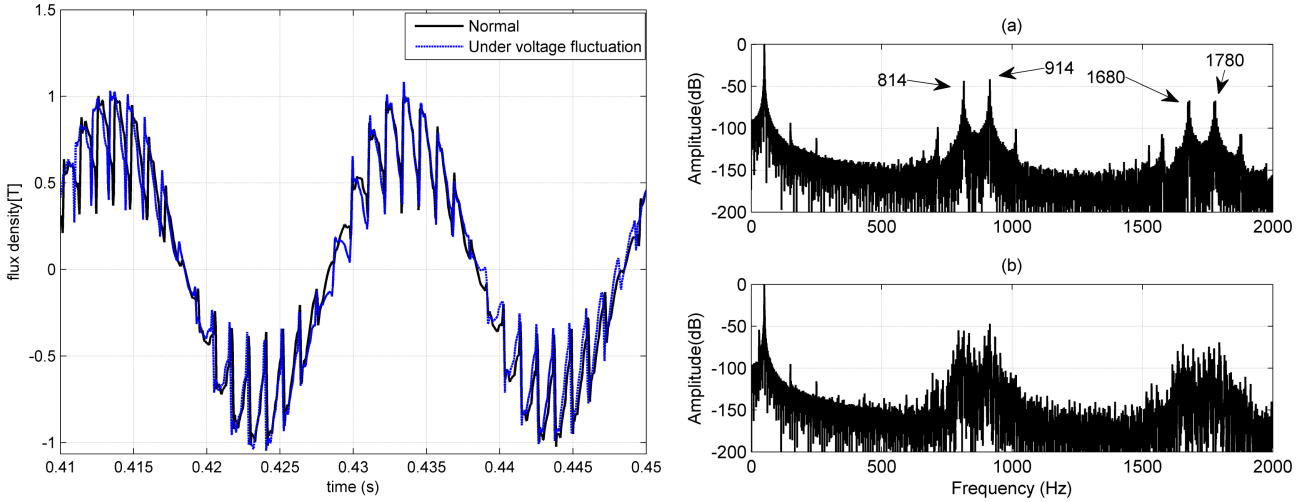

Fig. 7. (Color online) Magnetic flux density curves (left) and their frequency spectrum (right) at point A in two cases; (a) normal, (b) under fluctuated voltages ($f_m = 20$ Hz and $k = 0.05$).

the upper and lower flux density components, respectively. An increase in flux density is usually smaller than ΔB_m, because it also depends on phase angles of the flux density components in addition to their magnitudes. Under voltage fluctuation conditions, the upper components have opposite phase angles as compared to the lower components. Consequently, the total increase in the peak value of flux density due to fluctuated voltage is not the simple arithmetic sum of the individual components and may be smaller or equals to it:

$$B_{fluc} \leq 1 + \Delta B_m \tag{6}$$

where B_{fluc} is the normalized peak value of the flux density under voltage fluctuation conditions. As it can be seen in Fig. 7, the amplitudes of saturation harmonics under voltage fluctuation conditions have not changed significantly (as compared to the normal operation).

Voltage fluctuations have two important characteristics: the frequency of fluctuations (modulation frequency) and the magnitude of fluctuations (modulation depth). Both these components that are significant in the adverse effects of voltage fluctuations make the disturbance pattern. The normal range of modulation frequency is from 5 Hz to 35 Hz and the normal range of modulation depth lies between 0.1 % to 7 % [22].

To investigate the impact of modulation frequency on the magnetic circuit saturation, the modulation frequency is changed between 5 Hz to 35 Hz and the changes of the saturation third harmonic are investigated. The modulation depth is assumed 5 %. The variation of saturation third harmonic of the airgap flux density versus modulation frequency is shown in Fig. 8. The modulation depth is assumed 5 %. As it can be seen, the amplitude of

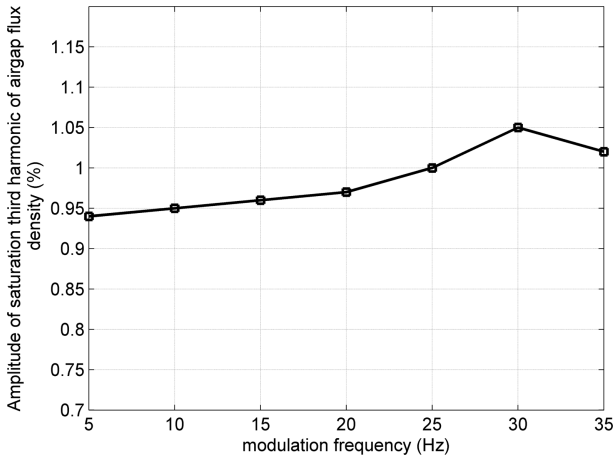

Fig. 8. Variation of saturation third harmonic of the airgap flux density versus modulation frequency ($k_m = 0.05$).

saturation harmonic has not changed significantly and varies between 0.95 and 1.05. It peaks at 30 Hz. The 30 Hz is one of the natural frequencies of the state matrix of linearized model of the simulated induction motor [6]. For the adverse condition of modulation frequency i.e. 30 Hz, the modulation depth is changed from 0.1 % to 7 % and variation of saturation third harmonic of the airgap flux density is obtained and shown in Fig. 9. As it can be seen, the amplitude of saturation harmonics under voltage fluctuation conditions varies between 0.97 and 1.08. The higher the modulation depth, the greater is the amplitude of saturation third harmonic. Based on these, it can be concluded that normal range of voltage fluctuations rarely makes whole magnetic circuit saturation.

Figure 10 shows flux density distribution of the simulated motor under normal and voltage fluctuation condi-

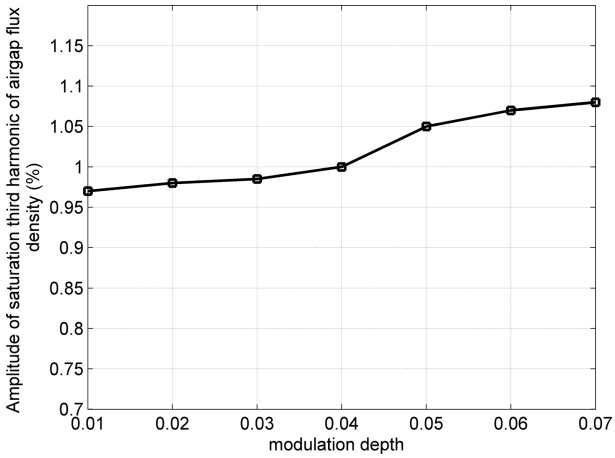

Fig. 9. Variation of saturation third harmonic of the airgap flux density versus modulation depth ($f_m = 30$ Hz).

tions. For this motor, the peak values of the flux density in the stator and rotor teeth are designed to be around 1.5 T. As seen, fluctuated voltages cause a slightly increase in the flux density values in some regions, especially in the stator teeth. Since this saturation does not cover the whole magnetic circuit and occurs only in some particular regions of rotor and stator teeth, it is called local saturation. The most important effect of local saturation is the change of locations of hot spot points within the core [23].

5. Experimental Results

In this section, the numerical results are validated under laboratory conditions. A 61704-chroma programmable AC source supplies 1.1 kW induction motor. To vary the load conditions, a 1.5 kW dc generator is coupled by a belt and pulley to the tested motor. An encoder is fastened to the shaft of the motor as an angular speed sensor to measure and records the speed changes versus time. In the data conditioning board, 3 LEM-LA-100-P and 5CSNE151 Honeywell current transducer sensors are used. All data is

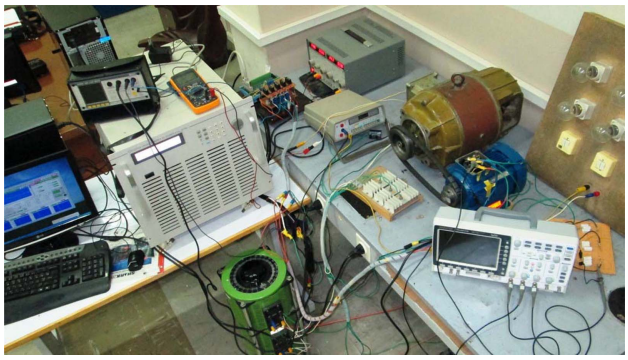

Fig. 11. (Color online) Overview of the complete experimental setup.

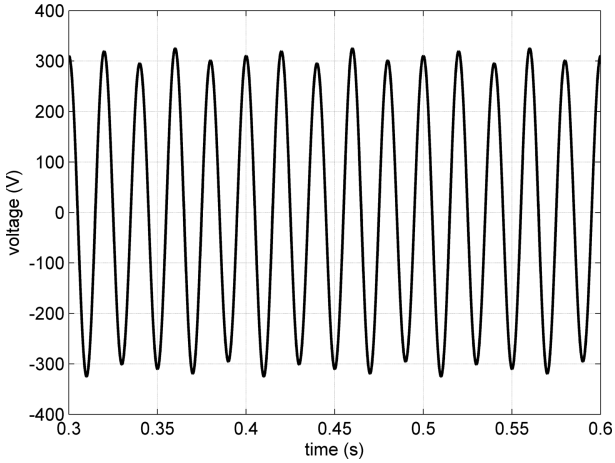

Fig. 12. Stator voltage of phase A ($f_m = 20$ Hz and $k = 0.05$).

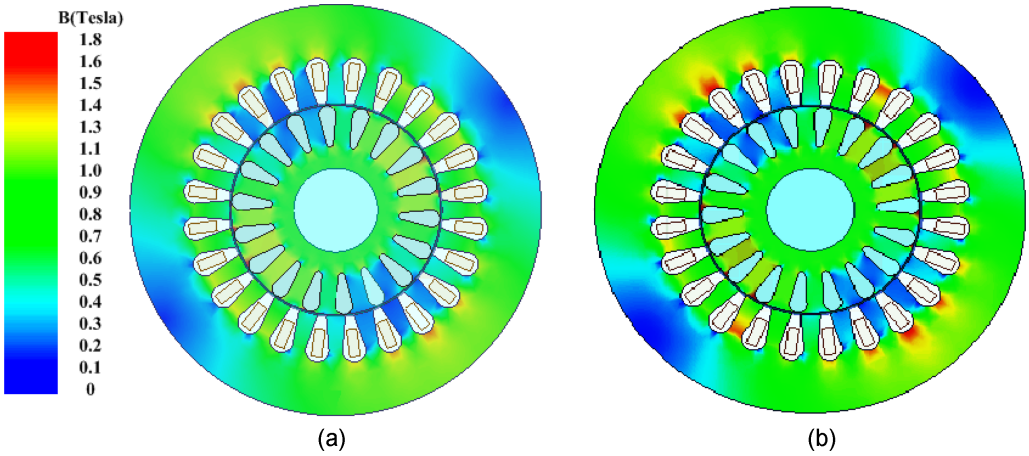

Fig. 10. (Color online) Steady state distribution of the magnetic flux density in two cases; (a) normal, (b) under voltage fluctuation conditions ($f_m = 20$ Hz and $k = 0.05$).

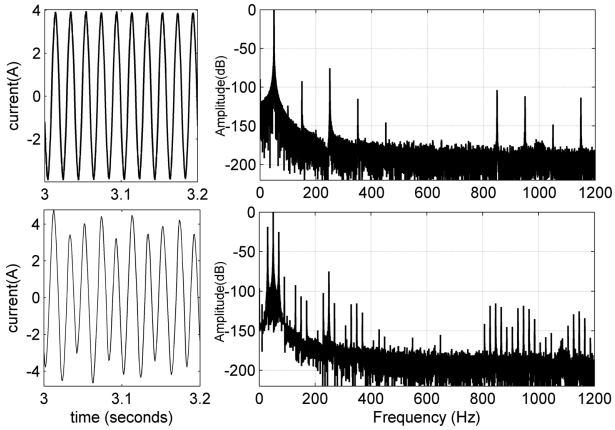

Fig. 13. Measured current in normal and under voltage fluctuation conditions ($f_m = 20$ Hz and $k = 0.05$).

acquired and transferred to a PC using the PCI-1710HG Advantech DAQ card. Figure 11 shows the overview of the complete experimental setup.

The induction motor is subjected to voltage fluctuations with modulation frequency of 20 Hz and modulation depth of 5 %. Figure 12 shows the stator voltage of phase A under voltage fluctuation conditions.

The waveforms captured in Fig. 13, show the measured stator current and their frequency spectrums under normal (top) and voltage fluctuation conditions (bottom). The slot and saturation harmonics can be clearly seen in the both normalized frequency spectrums while the upper and lower frequency components around each harmonics are only observed under voltage fluctuation conditions. Some additional harmonics can also be seen in the frequency spectrum under voltage fluctuation conditions. According to [5], variations of motor speed due to the voltage fluctuations result in the appearance of these additional components. Comparison of Fig. 4 and Fig. 13 depicts that the simulation results matches well with the experimental ones.

To obtain the flux density at stator tooth, a search coil with four turns is wounded around one of the motor stator tooth. The stator tooth flux density is the time integration of the induced voltage over this search coil. The search coil induced voltage and stator tooth flux density are shown in Fig. 14. The jagged waveform of the search coil voltage indicates the slotting effect. Furthermore, peak value of stator tooth flux density is about 1.24 T which is lower than the knee point of the magnetization curve of motor laminated iron. This fact proves that voltage fluctuations with normal range do not cause whole saturation of motor magnetic circuit.

Finally, the experimental waveforms of the motor speed is given in Fig. 15 and compared with the speed fluc-

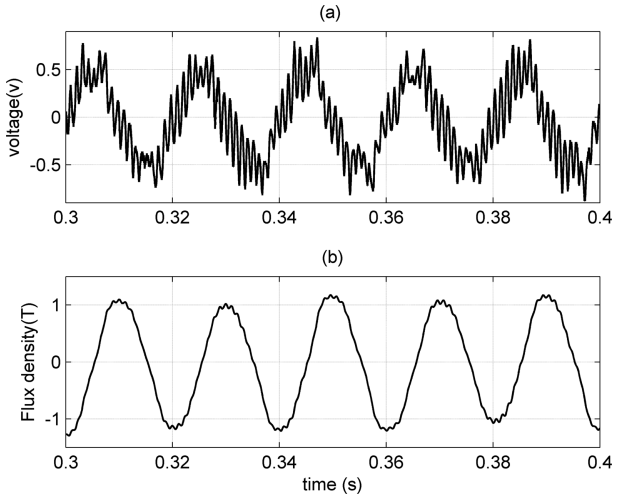

Fig. 14. Measured voltage and stator tooth flux density under voltage fluctuation conditions ($f_m = 20$ Hz and $k = 0.05$).

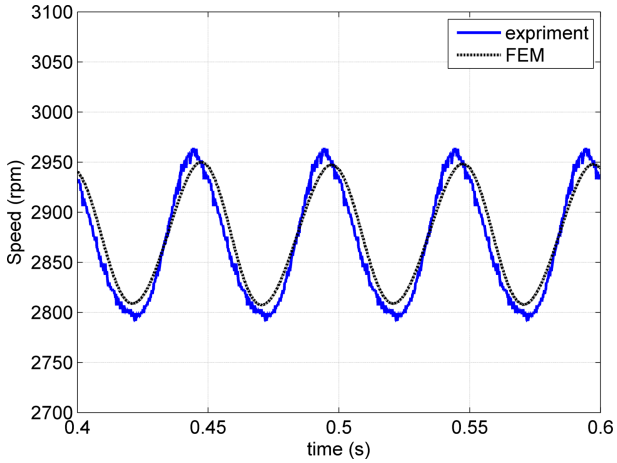

Fig. 15. (Color online) Measured speed fluctuations under voltage fluctuation conditions ($f_m = 20$ Hz and $k = 0.05$).

tuations obtained by FEM. A good correlation can be seen between the FEM and experimental results.

6. Conclusion

In this paper, finite element analysis has been conducted for the three phase induction motor to obtain the air gap flux component under voltage fluctuation conditions. A detailed analysis of the magnetic saturation based on saturation harmonics is presented. To investigate the impact of different characteristics of voltage fluctuations on the magnetic circuit saturation, the modulation depth and frequency are changed within normal range. During voltage fluctuation conditions, the airgap flux density has some extra frequency components as compared to pure sinusoidal supply. The maximum effect of each component

is proportional to its amplitude and phase angle. Under voltage fluctuation conditions, the upper components (interharmonics) have opposite phase angles as compared to the lower components (subharmonics) and consequently, the total increase in the peak value of flux density due to fluctuated voltage is small. Based on simulations, it is concluded that normal range of voltage fluctuations rarely causes whole magnetic circuit saturation, but it may create local saturation in the motor stator teeth. To validate the simulation results, an experimental test was conducted. A search coil was used to capture the stator tooth flux density. It was measured that, peak value of tooth flux density is lower than the knee point of the magnetization curve of motor laminated iron. Good correlations exist between measured parameters such as motor current and speed and same parameters obtained from simulations.

References

[1] H. Moghadam Banayem, A. Doroudi, and M. Poormonfared Azimi, Electric Power Components and Systems **43**, 412 (2015).
[2] Kyung-Won Jeon, Yong-Jae Kim, and Sang-Yong Jung, J. Magn. **18**, 212 (2013).
[3] R. H. C. Palácios, I. N. da Silva, A. Goedtel, and W. F. Godoy, Electr. Power Syst. Res. **127**, 249 (2015).
[4] K. Komeza and M. Dems, IEEE Trans. Ind. Electron. **59**, 2934 (2012).
[5] S. Tennakoon, S. Perera, and D. Robinson, IEEE Trans. Power Delivery **23**, 1207 (2008).
[6] M. GhasemiNezhad, A. Doroudi, and S. Hosseinian, International Power System Conference (PSC), Teharn, Iran (2009).
[7] M. GhasemiNezhad, A. Doroudi, and S. H. Hosseinian, Amirkabir Int. J. Electr. Electron. Eng. **44**, 53 (2012).
[8] J. Baptista, J. Gonçalves, S. Soares, A. Valente, R. Morais, J. Bulas-Cruz, and M. J. Reis, Electrical Machines (ICEM), 2010 XIX International Conference on, IEEE (2010) pp 1-6.
[9] P. Gnaciński and M. Pepliński, IET Electric. Power Appl. **8**, 287 (2014).
[10] M. Ghaseminezhad, A. Doroudi, S. H. Hosseinian, and A. Jalilian, IET Generation, Transmission & Distribution. **11**, 512 (2017).
[11] C. Lee, Trans. Am. Ins. Electr. Eng. **80**, 597 (1961).
[12] B. Chalmers and R. Dodgson, IEEE Trans. Power Appar. Syst. (1971) pp 564-569.
[13] X. Tu, L.-A. Dessaint, R. Champagne, and K. Al-Haddad, IEEE Trans. Ind. Electron. **55**, 2798 (2008).
[14] J. P. G. de Abreu and A. Emanuel, 2001 IEEE Industrial and Commercial Power Systems Technical Conference. Conference Record (Cat. No. 01CH37226), IEEE (2001) pp 105-114.
[15] R. Dugan, M. F. McGranaghan, and H. W. Beaty, Electric Power Systems Quality, McGraw-Hill (2002).
[16] M. Amrhein and P. T. Krein, IEEE Trans. Energy Convers. **25**, 339 (2010).
[17] J. Cheaytani, A. Benabou, A. Tounzi, M. Dessoude, L. Chevallier, and T. Henneron, IEEE Trans. Magn. (2015) pp 1-4.
[18] J.-J. Lee, Y.-K. Kim, H. Nam, K.-H. Ha, J.-P. Hong, and D.-H. Hwang, IEEE Trans. Magn. **40**, 762 (2004).
[19] S. Nandi, IEEE Trans. Ind. Appl. **40**, 1058 (2004).
[20] Y. Liao and T. A. Lipo, Electric Machines and Power Systems **22**, 155 (1994).
[21] G. Bottiglieri, A. Consoli, and T. A. Lipo, IEEE Trans. Energy Convers. **22**, 819 (2007).
[22] General guide on harmonics and interharmonics measurements for power supply systems and equipment connected thereto, IEC 61000-4-7.
[23] J. Faiz and B. M. Ebrahimi, Prog. Electromagn. Res. **64**, 239 (2006).